Recl. Trav. Chim. Pays-Bas **113**, 201–208 (1994)
SSDI 0165-0513(94)00004-L

0165-0513/94/04201–08$07.00

Surface monolayers and aqueous bilayers of single-chain ammonium amphiphiles which contain benzylideneaniline and salicylideneaniline units [1]

Taisei Nishimi, Yuichi Ishikawa, Reiko Ando and Toyoki Kunitake *

Department of Chemical Science and Technology, Faculty of Engineering, Kyushu University, Fukuoka 812, Japan
(Received October 12, 1993)

Abstract. The assembling properties of single-chain ammonium amphiphiles containing benzylideneaniline and salicylideneaniline units as rigid segments in the formation of aqueous bilayers, cast multi-bilayers, and surface monolayers were studied. Electron microscopy indicated that aggregate morphologies observed in water, such as vesicles and fibers, were dependent on the nature of the aromatic unit and the alkyl-chain length of the component amphiphiles. The patterns of molecular assembly in bilayers were examined by absorption spectroscopy of aqueous bilayers and X-ray diffraction of cast multi-bilayer films. The patterns were virtually identical to those of the corresponding azobenzene bilayers, and commonly determined by combinations of alkyl-chain lengths. This alkyl-chain combination was crucial for formation of stable surface monolayers.

1. Introduction

Since the first report of a totally synthetic bilayer membrane[2], spontaneous bilayer formation has been described for a large variety of amphiphiles[3]. Conventional monoalkyl surfactants usually form fluid micelles in dilute aqueous solution. However, when some aromatic groups are introduced as rigid segments, monoalkyl surfactant molecules become better oriented in aqueous aggregates to produce stable bilayer assemblies[4]. We have reported that aggregate morphologies are closely related to the geometry of a rigid segment involved in an extensive series of single-chain ammonium amphiphiles[5]. Azobenzene-containing ammonium amphiphiles (**1**: $C_nAzoC_mN^+$) belong to this class. Their ability to form bilayers spontaneously and their mode of molecular packing in the aggregate depend on their alkyl-chain lengths[6,7]. Figure 1 shows schematic illustrations of the representative molecular packing in the azobenzene bilayer. Some of these structures have been confirmed by single-crystal X-ray diffraction studies[8,9]. These packing modes affect the rate of photo-isomerization and the efficiency of energy migration in the aqueous bilayer system[10].

The azobenzene amphiphiles also form monolayers at the air–water interface and their molecular orientation in the monolayers displays some resemblance to that of the corresponding aqueous bilayer[11–13].

The correspondence observed between the molecular structure and the mode of molecular assembly should be valuable in designing novel molecular aggregates. It is important to find generalized structure–assembly relationships. For this purpose, we replaced the azobenzene unit with geometrically similar benzylideneaniline (**2**: $C_nBenanC_mN^+$) or salicylideneaniline units (**3**: C_nSalan-C_mN^+) and examined their aggregate structures.

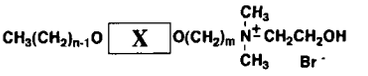

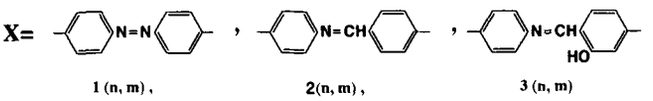

1 (n, m), 2(n, m), 3 (n, m)

Related benzylideneaniline amphiphiles **4** and **5** were systematically synthesized some years ago, and their aggregation behavior (aggregate morphology, aggregation number and critical aggregate concentration) was examined in relation to their chemical structure[4]. The nucleophilic reaction toward the benzylideneaniline unit in bilayer membranes was examined later[14]. This reactivity was influenced by the membrane physical state and the distance of the reacting functional group from the membrane surface. However, the exact packing mode of these bilayer membranes was not clear at that time. In order to make a more precise comparison of molecular alignments with those of the azobenzene bilayer, we synthesized novel amphiphiles **2**, in which only the azobenzene unit is replaced by the benzylideneaniline unit. The molecular alignment of the salicylideneaniline bilayer **3** was reported briefly[15]. The present paper contains a fuller account and a structural comparison with the other bilayers.

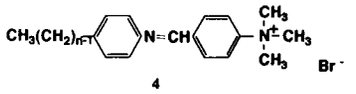

4

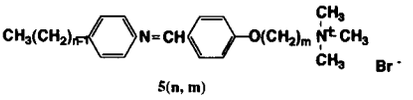

5(n, m)

2. Experimental

2.1. Materials

Ammonium amphiphiles **2** and **3** were prepared according to the routes in Eqns. 1–3. The structures of the intermediates and final products were confirmed by thin-layer chromatography (TLC), IR and ^{1}H-NMR spectroscopies, and elemental analysis. The melting point (uncorrected) was measured with a polarizing microscope, and the liquid–crystalline region is denoted by the arrow.

N-[4-[5-[(2-Hydroxyethyl)dimethylammonio]pentyloxy]benzylidene]-4-(dodecyloxy)aniline bromide **2***(12,5).* 4-Hydroxybenzaldehyde (0.5 g, 4.1 mmol) and 1,5-dibromopentane (4.7 g, 20.4 mmol) were dissolved in ethanol (100 ml) which contained 85% KOH (0.27 g, 5.7 mmol), and refluxed for 5 h. After cooling to room temperature, KBr was removed, and 4-(dodecyloxy)aniline (1.3 g, 4.2 mmol) in ethanol was added and refluxed for 2 h. Precipitates were collected at room temperature and recrystallized from ethanol to give *N*-[4(-5-bromopentyloxy)benzylidene]-4-(dodecyloxy)aniline as colorless powders; yield 21%; m.p. 85 → 115°C; TLC (silica gel, $CHCl_3$), R_f 0.68. The product (0.40 g, 0.75 mmol) and 2-(dimethylamino)ethanol (2.0 g, 22.5 mmol) were dissolved in benzene (50 ml) and refluxed for 20 h. After removing solvent and excess amine, the residue was recrystallized from a mixture of benzene and hexane to give colorless flakes of **2**(12,5); yield 64%; m.p. 145 → 243°C. ^{1}H NMR ($CDCl_3$) δ: 0.93, t, 2.9, C–CH_3; 1.30, m, 26.5, C–CH_2–C; 3.26, m, 12.7, CH_2–N^+–CH_3, C–CH_2–O); 3.93, t, 4.0, C–CH_2–O; 6.70–7.92, m, 8.0, phenyl; 8.38, s, 1.0, CH=N. Anal. calcd. for $C_{34}H_{55}N_2O_3Br$ (619.73): C 65.90, H 8.95, N 4.52; found: C 65.87, H 8.92, N 4.44%.

N-[4-[10-[(2-Hydroxyethyl)dimethylammonio]decyloxy]benzylidene]-4-(dodecyloxy)aniline bromide **2***(12,10).* This compound was prepared as a colorless powder in a manner similar to the synthesis of **2**(12,5); m.p. 140 → 220°C. ^{1}H NMR ($CDCl_3$) δ: 0.93, t, 3.5, C–CH_3; 1.30, m, 36.9, C–CH_2–C; 3.26, m, 11.6, CH_2–N^+–CH_3, C–CH_2–O; 3.93, t, 4.6, C–CH_2–O; 6.80–7.95, m, 8.0, phenyl; 8.43, s, 1.1, CH=N. Anal. calcd. for $C_{39}H_{65}N_2O_3Br$ (689.86): C 67.90, H 9.50, N 4.06; found: C 67.67, H 9.52, N 3.90%.

N-[4-[10-[(2-Hydroxyethyl)dimethylammonio]decyloxy]benzylidene]-4-(octyloxy)aniline bromide **2***(8,10).* This compound was prepared as a colorless powder in a manner similar to the synthesis of **2**(12,5); m.p. 165 → 215°C. ^{1}H NMR ($CDCl_3$) δ: 0.93, t, 2.3, C–CH_3; 1.30, m, 27.7, C–CH_2–C; δ 3.26, m, 10.4, CH_2–N^+–CH_3, C–CH_2–O; 3.93, t, 4.6, C–CH_2–O; 6.89–7.92, m, 8.0. phenyl; 8.43, s, 1.2, CH=N. Anal. calcd. for $C_{35}H_{57}N_2O_3Br$ (633.75): C 66.33, H 9.07, N 4.42; found: C 66.58, H 9.14, N 4.32%.

N-[4-[5-[(2-Hydroxyethyl)dimethylammonio]pentyloxy]salicylidene]-4-(dodecyloxy)aniline bromide **3***(12,5).* 2,4-Dihydroxybenzaldehyde (1.0 g, 7.2 mmol) and 1,5-dibromopentane (8.3 g, 36 mmol) were dissolved in ethanol (200 ml) which contained 0.48 g (7.2 mmol) of 85% KOH, and refluxed for 5 h under nitrogen atmosphere. After removal of KBr, 4-(dodecyloxy)aniline (2.2 g, 7.1 mmol) in ethanol was added and stirred for 2 h at room temperature. Resulting precipitates were collected, purified on a silica-gel column using chloroform as developing solvent, and recrystallized from hexane/benzene to give *N*[4-(5-bromopentyloxy)salicylidene]-4-(dodecyloxy)aniline as pale yellow plates; yield 62%; m.p. 63 → 131°C; TLC (silica gel, $CHCl_3$) R_f 0.67. ^{1}H NMR ($CDCl_3$) δ: 0.91, t, 4.2, C–CH_3; 1.30, m, 26.7, C–CH_2–C; 3.35, t, 1.9, C–CH_2–Br; 3.93, t, 3.6, C–CH_2–O; 6.40–7.09 m, 7.0, phenyl; 8.38, s, 0.9, CH=N. This product and 2-(dimethylamino)ethanol (4.0 g, 45 mmol) were dissolved in benzene (100 ml), and refluxed for 6 h. After the solvent and excess amine were removed, the residue was recrystallized from benzene to give yellow prisms of **3**(12,5) in 65% yield; m.p. 126 → 263°C; ^{1}H NMR ($CDCl_3$) δ: 0.93, t, 3.3, C–CH_3; 1.30, m, 25.6, C–CH_2–C; 3.26–3.93, m, 16.7, CH_2–N^+–CH_3, C–CH_2–O; 6.40–7.15, m, 7.0 phenyl, 8.43, s, 1.0, CH=N. Anal. calcd. for $C_{34}H_{55}N_2O_4Br$ (635.73): C 64.24, H 8.72, N 4.41; found: C 64.10, H 8.66, N 4.46%.

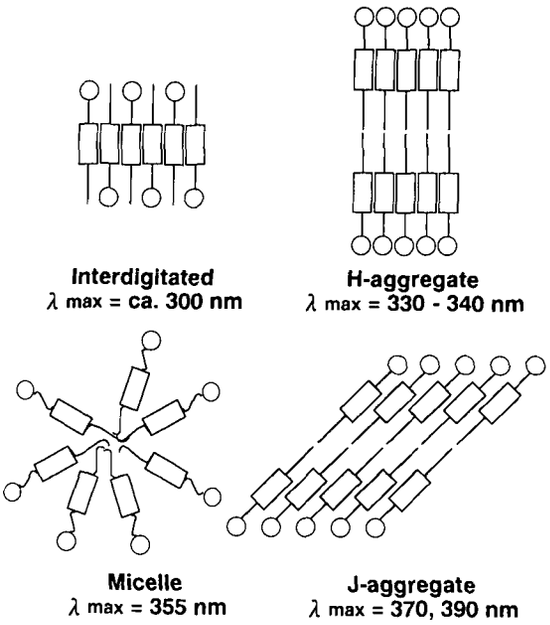

Figure 1. Schematic modes of aggregation of azobenzene-containing amphiphiles **1** *and absorption maxima of the aggregates.*

N-[4-[5-[(2-Hydroxyethyl)dimethylammonio]decyloxy]salicylidene]-4-(dodecyloxy)aniline bromide **3***(12,10).* This compound was prepared as a yellow powder in a manner similar to the synthesis of **3**(12,5); m.p. 113 → 240°C. ^{1}H NMR ($CDCl_3$) δ: 0.89, t, 3.0, C–CH_3; 1.30, m, 34.1, C–CH_2–C; 3.31–3.92, m, 16.3, CH_2–N^+–CH_3, C–CH_2–O; 6.40–7.15, m, 7.0, phenyl; 8.41, s, 1.0, CH=N. Anal. calcd. for $C_{39}H_{65}N_2O_4Br$ (705.86): C 66.36, H 9.28, N. 3.97; found: C 66.09, H 9.21, N 3.90%.

N-[4-[10-[(2-Hydroxyethyl)dimethylammonio]decyloxy]salicylidene]-4-(octyloxy)aniline bromide **3***(8,10).* This compound was prepared as a yellow powder in a manner similar to the synthesis of **3**(12,5); m.p. 145 → 220°C; ^{1}H NMR ($CDCl_3$) δ: 0.93, t, 2.4, C–CH_3; 1.30, m, 26.2, C–CH_2–C; 3.26–3.93, m, 15.2, CH_2–N^+–CH_3, C–CH_2–O; 6.40–7.15, m, 7.0, phenyl; 8.41, s, 1.0, CH=N. Anal. calcd. for $C_{35}H_{57}N_2O_4Br$ (649.75): C 64.70, H 8.84, N 4.31; found: C 64.69, H 8.75, N 4.29%.

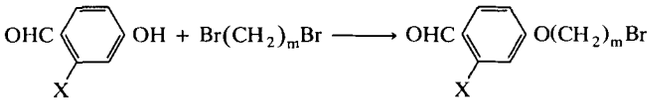

(1)

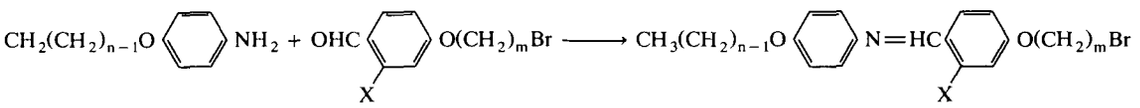

(2)

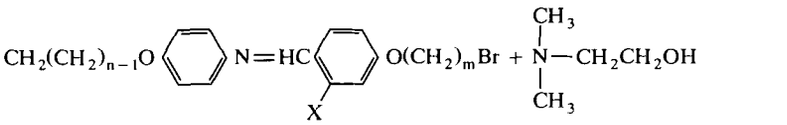

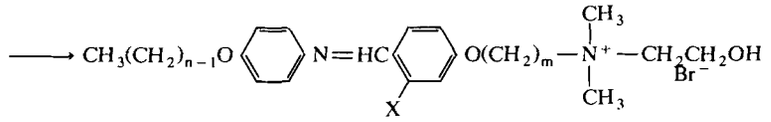

(3)

2.2. *Characterization of aqueous bilayers*

Aqueous stock solutions (10 mM) of **2** and **3** were prepared by sonication with a Branson Sonifier 185 (microtip, sonic power 40) and by heating, respectively. Differential-scanning-calorimetry (DSC) measurements were carried out with a Seiko Instrument SSC-560 instrument. The stock solutions were sealed in silver pans and temperature scan was repeated from 5 to 80°C at a rate of 1°C/min. The endothermic peak top was adopted as the phase transition temperature (T_c), and the enthalpy change (ΔH) was estimated from the peak area by the baseline method. The entropy change (ΔS) was calculated as $\Delta S = \Delta H / T_c$.
Absorption spectra were measured in 1-mm quartz cells with a Hitachi 124 UV-Vis spectrometer. Stock solutions of **2** and **3** were diluted to 1.0 mM with deionized water and acetate buffer [pH 5.2, μ 0.01 (CH_3COOK)], respectively. The salicylideneaniline group must remain undissociated in this pH range[15]. The temperature-dependent spectra were measured at every 10°C in the heating cycle. The samples were kept at temperatures of measurement for 10 min to ensure thermal equilibration.
Aggregate morphologies of these bilayers were observed by transmission-electron micrography (Hitachi H-600). Stock solutions (10 mM) were applied to carbon-coated copper meshes and air-dried at room temperature. Aqueous uranyl acetate was then placed on the copper mesh and air-dried.

2.3. *Characterization of cast films and surface monolayers*

Self-supporting films (1.5×2.0 cm) were obtained from the amphiphiles by casting of stock solutions (100 mM, 500 μl) on Teflon

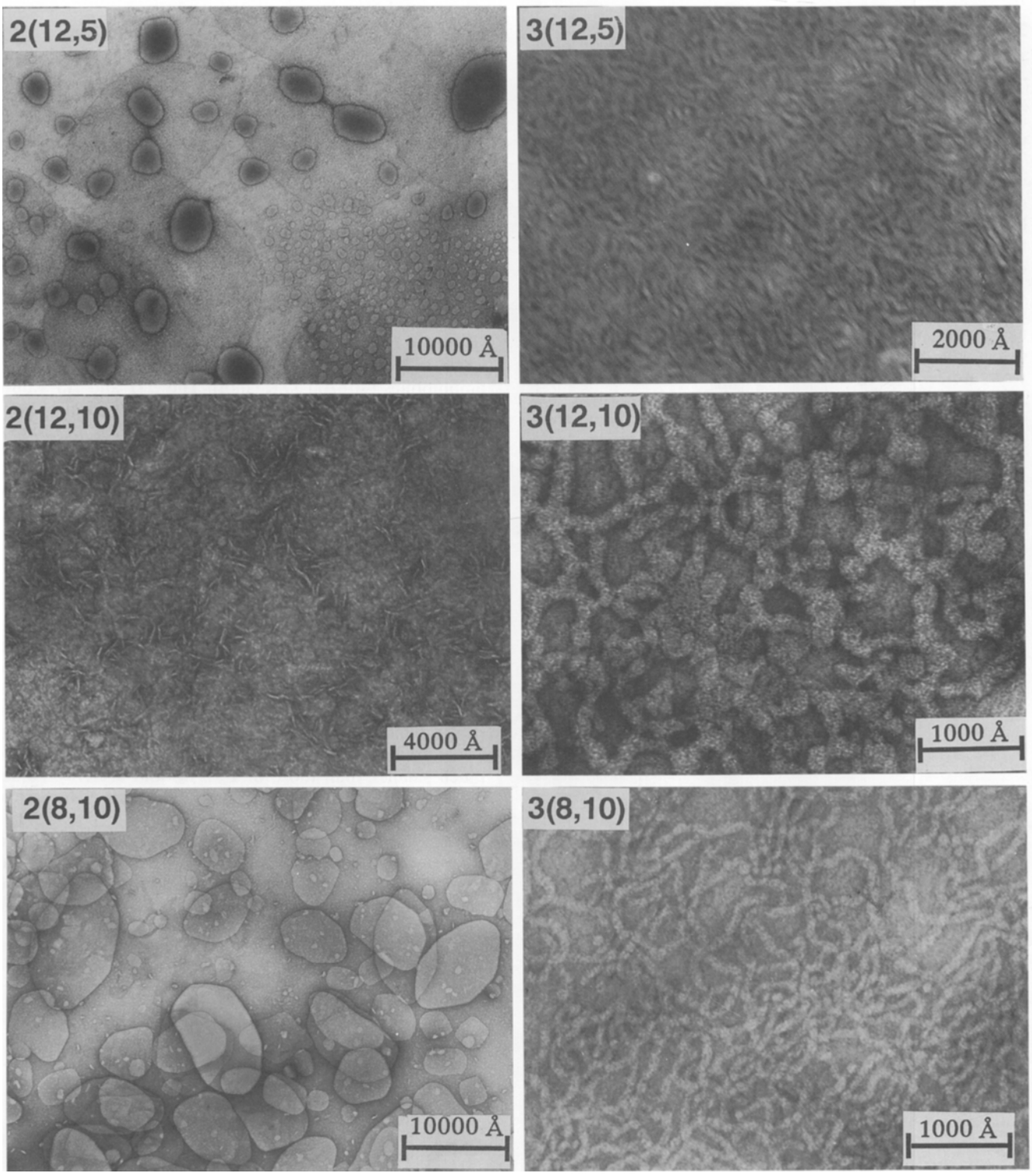

Figure 2. Electron micrographs of aqueous aggregates (10 mM) of 2 and 3. Stained by uranyl acetate.

sheets at room temperature. X-ray diffraction (XRD) patterns of these films were obtained by the reflection method ($2\cdot\theta-\theta$ scan) with a Rigaku RAD-R-32 diffractometer at room temperature. The CuK_α beam was taken out via a graphite monochrometer.
The spreading solutions for monolayers were prepared in a 7:1:2 mixture (by volume) of benzene, ethanol and dichloromethane. The water used as subphase was purified by the Milli-Q system (Millipore Ltd.). Pressure-area isotherms of surface monolayer (π-A curves) were obtained with a computer-controlled film balance (Sanesu Keisoku FSD-20) at 20 ± 2°C. The monolayers were compressed at a rate of 0.04 mm/s. Absorption spectra of the monolayer were obtained by a photodiode-array-equipped spectrometer (Otsuka Electronics, model MCPD-110). The tip of a Y-type optical fiber was fixed vertically at a position 2–3 mm above the water surface. A tilted black plate was placed in the Langmuir trough below the optical fiber.

3. Results and Discussion

3.1. Electron microscopy of aqueous dispersions

The six compounds we employed in this study can be dispersed in water either by sonication or by warming. These transparent dispersions were subjected to electron microscopic observation. As shown in Figure 2, aggregate structures are found for all the specimens; however, the bilayer structure is generally not so well developed as had been observed for typical bilayer membranes. An aqueous dispersion of **2**(12,5) contained single-walled vesicular aggregates, whose walls are, however, much thicker than expected from the single-bilayer thickness. Short fibrous aggregates with diameters of 60–70 Å are found for a dispersion of **2**(12,10). Aqueous **2**(8,10) produced large structureless aggregates. In closely related series of benzylideneaniline amphiphiles **4** and **5**, the bilayer structure was similarly observed for aqueous dispersions by electron micoscopy.
In the case of aqueous **3**(12,5), fibrous aggregates (diameter *ca.* 150 Å) are formed. Elongation of the spacer methylene as in **3**(12,10) gives rise to trains of spheres (diameter *ca.* 150 Å). **3**(8,10) produces irregular fibers (diameter *ca.* 150 Å).

3.2. Molecular alignment in aqueous dispersions

Aqueous bilayer dispersions display phase transitions from the gel to liquid crystalline state due to side-chain melting. DSC is one of the most effective means to detect this phase transition. DSC thermograms of aqueous **2** and **3**

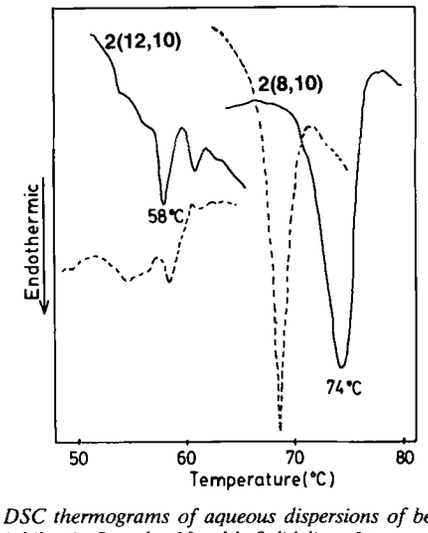

Figure 3. DSC thermograms of aqueous dispersions of benzylideneaniline amphiphiles 2. Sample, 10 mM. Solid line, 1st scan. Broken line, 2nd scan.

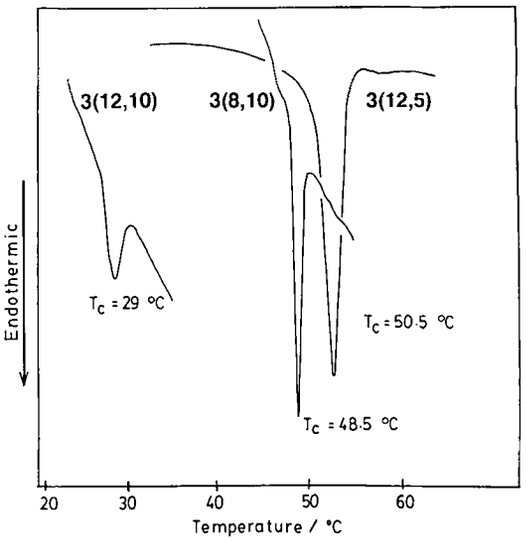

Figure 4. DSC thermograms of aqueous dispersions of salicylideneaniline amphiphiles 3. Sample, 10 mM.

are shown in Figure 3 and Figure 4, respectively. The thermodynamic parameters obtained therefrom are compared with those of the azobenzene bilayers (**1**) in Table I. Endothermic peaks were observed for all the samples in the range of 5–80°C except for **2**(12,5).
In our former compilation[16], the entropy change due to the phase transition of bilayers of single-chain amphiphiles falls in the range of 25 to 75 J/K · mol in most cases and was much smaller than those for double-chain amphiphiles (70–200 J/K · mol). The ΔH and ΔS values for aqueous **3**(12,5) are too large to be a typical bilayer-phase transition. These values imply complete disintegration of the crystalline bilayer structure. Thus, the particular combination of the alkyl-chain length included in **2**(12,5) and **3**(12,5) appears not sufficient to maintain typical bilayer behavior. These results contrast with those for the corresponding azobenzene amphiphile **1**(12,5), which forms typical bilayer dispersions[6]. The stacking interaction of the azobenzene unit must be greater than those of the other two, giving rise to a stable bilayer assembly.
When the spacer methylene chain (c_m portion) was extended from C_5 to C_{10}, the DSC data became more appropriate for the bilayer phase transition. Aqueous dispersions of **2**(12,10) and **3**(12,10) showed endothermic peaks typical of phase transition of aqueous bilayers. Phase transition parameters (T_c, ΔH, ΔS) of **3**(12,10) are much smaller than those of **1**(12,10) and **2**(12,10). Aqueous bilayers **2**(8,10) and **3**(8,10) also showed endothermic peaks.
In the case of benzylideneaniline bilayers of **2**(12,10) and **2**(8,10), the second DSC scans gave peaks quite different from those of the first scans. The transition temperature became lower or the peak shape broadened (Figure 3,

Table I Phase transition data of aqueous dispersions.

Amphiphile	T_c (°C)	ΔH (KJ/mol)	ΔS (J/K·mol)
1(12,5)	32.0	14.0	46
2(12,5)	n.d.[a]	–	–
3(12,5)	50.5	93.6	298
1(12,10)	56.0	20.2	61
2(12,10)	58.0	21.2	64
3(12,10)	29.0	9.6	32
1(8,10)	68.0	46.9	138
2(8,10)	74.0	59.3	171
3(8,10)	48.5	14.6	45

[a] n.d.: not detected.

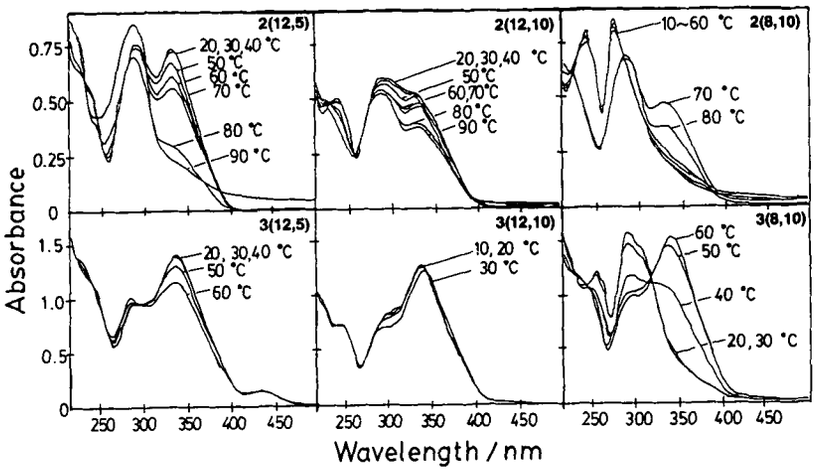

Figure 5. UV-visible absorption spectral changes of aqueous 2 and 3 in the heating process; 2, 1.0 mM in pure water; 3, 1.0 mM in acetate buffer [pH 5.6, μ 0.01 (CH_3COOK)].

broken line). These anomalies may be ascribed to hydration and/or hydrolysis of the benzylideneaniline unit during the DSC measurement (Eqn. 4), as we have reported for a related bilayer[14]. The UV-spectral change of the aqueous dispersion at elevated temperatures (see below) is consistent with this presumption.

$$-CH{=}N- + H_2O \longrightarrow -CH(OH)-NH- \longrightarrow -CHO + H_2N- \quad (4)$$

No chemical change was observed for the salicylideneaniline counterparts. The different chemical stabilities of these two bilayer systems can be explained by the presence/absence of intramolecular hydrogen bonding. The salicylideneaniline unit forms an intramolecular hydrogen bond between hydroxylic proton and the Schiff base nitrogen (-CH=N · · · H-O) so that the Schiff base is chemically stabilized. The stabilization is not possible for the benzylideneaniline unit, and the water molecule can attack the Schiff base easily.

A similar chemical stabilization has been reported for salicylideneaniline-containing liquid crystals[17].

3.2. Chromophore alignment in aqueous dispersion

As mentioned in the introduction, azobenzene bilayers **1** show large absorption spectral shifts that are induced by differing modes of azobenzene stacking in bilayers[6]. We applied this spectral technique to aqueous dispersions of **2** and **3**. Figure 5 summarizes absorption spectra obtained at various temperatures in the heating process.

In molecularly dispersed solutions of **1**, **2**, and **3** in ethanol λ_{max} attributed to the π–π^* transition along the long axes of the chromophores[18] are found at 355, 335, and 345 nm respectively, independent of the alkyl-chain length in each series. It is known that azobenzene bilayer **1**(12,5) form J aggregates with red-shifted absorption at 370 and 390 nm in the gel state[6]. However, aqueous bilayers of **2**(12,5) and **3**(12,5) did not display significant spectral shifts relative to their molecular species. These amphiphiles did not show peaks for gel-to-liquid crystalline-phase transition in the DSC measurement at 10 mM. These facts suggest either that less ordered aggregates like micelles are formed under these conditions, or that

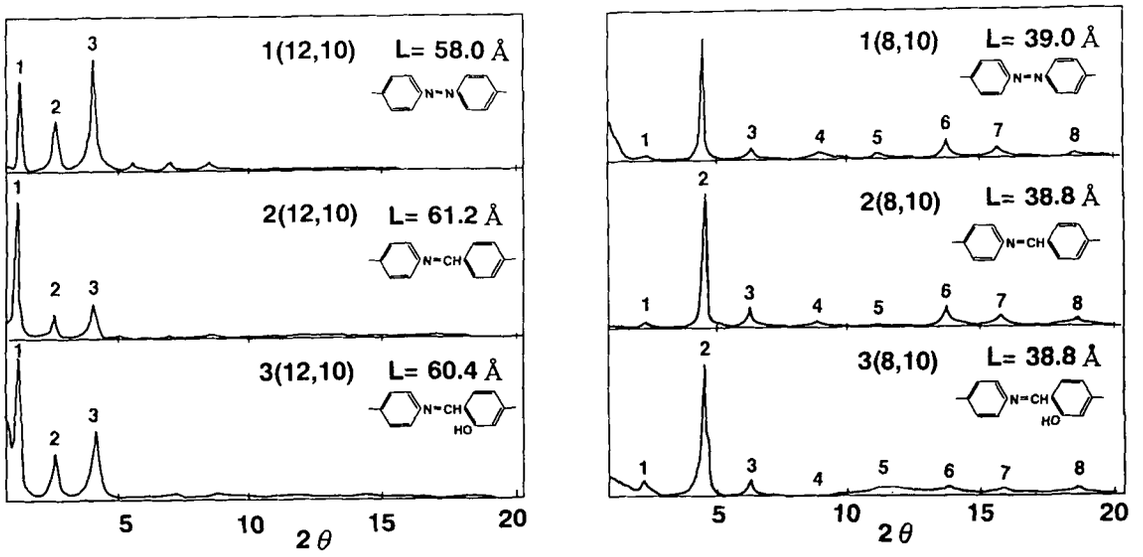

Figure 6. Reflection-X-ray diffraction of cast films of bilayer-forming amphiphiles 1, 2 and 3.

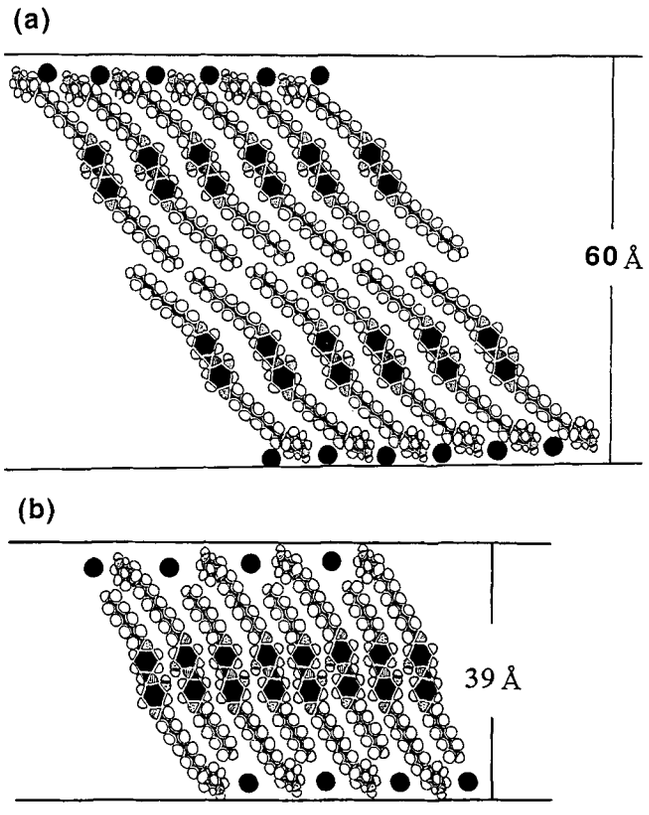

Figure 7. Patterns of aggregation of single-chain amphiphiles, 1, 2 and 3. The patterns (a) and (b) apply to amphiphiles possessing alkyl chain combinations of (12,10) and (8,10) respectively. The particular CPK models used for the illustrations are 3(12,10) and 3(8,10).

these aggregates remain in the liquid–crystalline state in the temperature range employed, thus excluding the chromophore interaction. The 335-nm peak of **2**(12,5) diminished irreversibly at temperatures above 80°C. This must be caused by hydration/hydrolysis of the Schiff base as discussed above in connection with DSC data.

Azobenzene bilayer **1**(12,10) displays a blue shift (at 330 nm) of the π–π^* transition due to the parallel chromophore stacking. In the case of related benzylideneaniline bilayer **2**(12,10), the π–π^* transition along the chromophore long axis is broadened due to overlapping with a shorter wavelength peak at 285 nm, and is observed as a shoulder peak at around 330 nm. Therefore the blue shift due to the chromophore stacking is not very distinctive. The spectral shape becomes identical with that of the monomer spectrum at 60–70°C, where the phase transition occurs. At still higher temperatures (80–90°C), the spectral intensity is diminished, probably due to irreversible hydrolysis/hydration of the chromophore.

Bilayer **3**(12,10) gives λ_{max} at 335 nm which is blue-shifted by 10 nm from that of the monomer species. The spectrum characteristic of the monomer species is seen upon phase transition at approximately 30°C. This change is reversible and no chemical changes proceed in this temperature range.

Bilayers **2**(8,10) and **3**(8,10) show large blue shifts in the gel state (at low temperatures) relative to their monomer species, as is the case with the azobenzene bilayer. These λ_{max}'s are located at 272 nm at 10–60°C and at 290 nm at 20–30°C, respectively. The large blue shifts observed are indicative of the interdigitated parallel stacking. At temperatures (70–80°C) above T_c, bilayer **2**(8,10) showed a monomer spectrum followed by an intensity decrease (hydration/hydrolysis). Bilayer **3**(8,10) gave monomer spectra at 50–60°C (T_c 48.5°C).

3.3. Molecular alignment in cast multibilayer films

The molecular alignment in bilayer membranes is more reliably determined by X-ray diffraction of cast films and single crystals. The details of the bilayer arrangement have been obtained for azobenzene bilayers **1**. We can deduce the molecular arrangement of **2** and **3** by comparing their X-ray diffraction patterns with those of **1**.

Cast films were prepared by spreading aqueous bilayer dispersions on solid supports. Absorption spectra of the cast films are similar to those of the corresponding aqueous dispersions in the crystalline state (at low temperatures). Therefore, it is assumed that the chromophore arrangement in aqueous dispersion and in cast film shows common features.

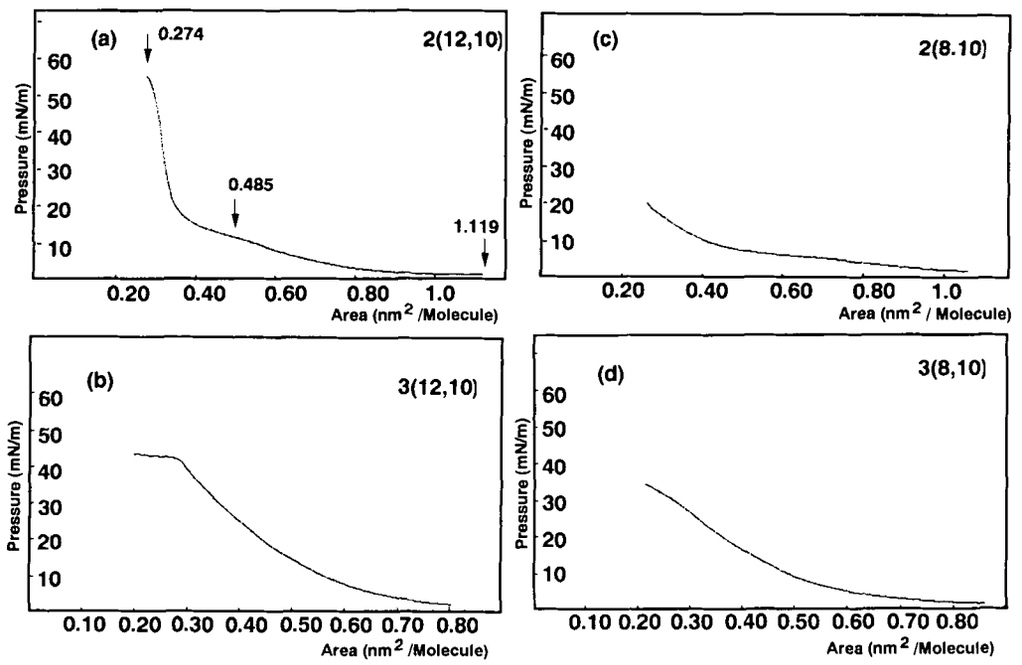

Figure 8. Surface-pressure–area isotherms of amphiphiles 2 and 3 on pure water at 20.0°C.

Reflection-X-ray diffraction patterns are given in Figure 6. Cast films of **1**(12,10), **2**(12,10), and **3**(12,10) display in common strong first- and third-order diffractions along with a weak second order diffraction. Their long spacings are 61.7, 61.2 and 60.4 Å, respectively. The extended molecular lengths of these compounds are estimated to be about 44 Å from the space-filling molecular model. The observed long spacings are in between the one-molecular length and the two-molecular length, and are satisfied by a tilted bilayer structure illustrated in Figure 7a. Rather small blue shifts (*ca.* 10 nm) observed in absorption spectroscopy are consistent with this chromophore arrangement.

The diffraction pattern is virtually identical for **1**(8,10), **2**(8,10), and **3**(8,10). This again indicates that the different kinds of chromophores do not produce significant differences in molecular packing. The XRD patterns are characterized by weak first-order peaks, very strong second-order peaks, and weak third- to eighth-order peaks with common long spacings of 38.8 Å. The extended molecular lengths are 39.0 Å and the layer thickness (long spacing) corresponds to the one-molecular length. The molecular arrangement in bilayer **1**(8,10) has been determined by single-crystal X-ray diffraction[8]. We can safely assume the same arrangement of **2**(8,10) and **3**(8,10), as shown in Figure 7b.

3.4. Formation and absorption spectra of surface monolayers

Monolayer properties of **2**(12,10), **3**(12,10), **2**(8,10), and **3**(8,10), which were confirmed to form aqueous bilayers as discussed above, were studied at the air–water interface. Pressure–area isotherms (π–A curves) and absorption spectra of monolayers are shown in Figure 8 and Figure 9, respectively.

The π–A curve of **2**(12,10) (Figure 8a) shows a transition from liquid expanded film to the condensed film during compression. The transition is accompanied by an absorption-spectral change from that of the monomeric species to that of the H aggregate. The latter spectrum is similar to that of the corresponding aqueous bilayer in the gel phase. Therefore, the transitions in aqueous bilayer and in surface monolayer must be essentially identical in terms

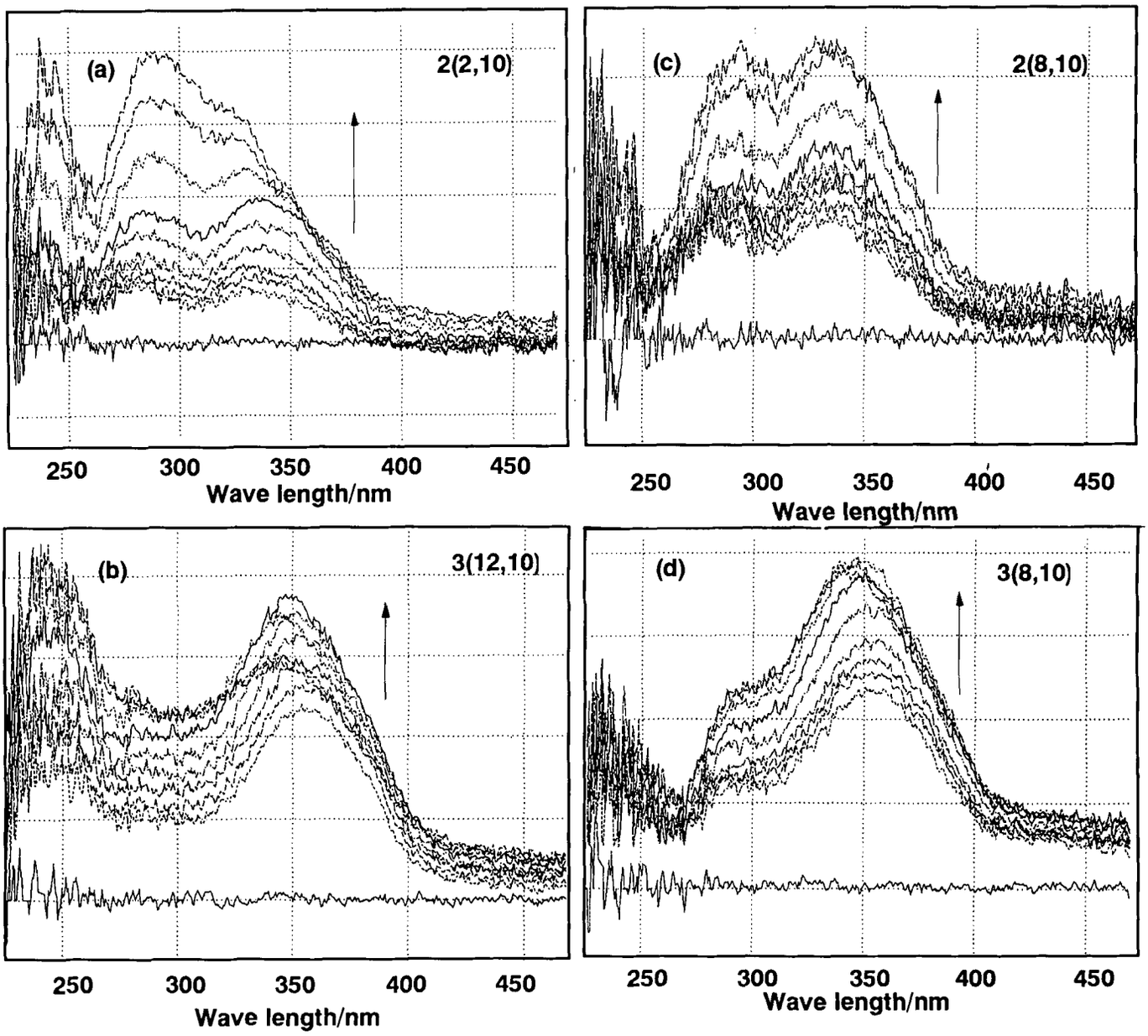

Figure 9. Absorption spectra of surface monolayers of 2 and 3 on pure water at 20°C. The spectral data were collected at every 2 min during the isotherm measurement of Figure 8. For example, the molecular areas designated in Figure 8a correspond to the 2nd, 8th and 10th runs of Figure 9a. The 1st spectral run was obtained prior to monolayer spreading.

of molecular orientation. A very similar situation has been found for azobenzene bilayer **1**(12,10)[11].

On the other hand, **3**(12,10) did not show such a transition at the air–water interface (Figure 8b). Compression to areas smaller than 30 nm^2/molecule produced a plateau and then caused collapse. The absorption pattern remained unchanged during the compression (Figure 9b). The stacking interaction of the salicylideneaniline unit is apparently smaller than those of the azobenzene and benzylideneaniline units and therefore, the monolayer of **3**(12,10) cannot form a condensed phase. The low T_c value of aqueous bilayer of **3**(12,10) relative to those of bilayers **1**(12,10) and **2**(12,10) supports this idea. In spite of geometrical similarity, different stacking interactions between **3** and **1** and **2** are noticeable in aqueous bilayers and in surface monolayers.

Neither **2**(8,10) nor **3**(8,10) formed condensed monolayers. A similar behavior has been observed for **1**(8,10). This azobenzene amphiphile forms an interdigitated bilayer assembly as an aqueous dispersion. The strong stacking characteristic of the interdigitated bilayer cannot be produced in surface monolayers, because all the head groups must stay in contact with water. Therefore, azobenzene amphiphile **1**(8,10) only forms a loosely aligned monolayer. The same situation is observed for **2**(8,10) and **3**(8,10), as is clear from the interdigitated structure of their aqueous bilayers and expanded phases and low collapse pressures in their π–A isotherms (Figures 8c and 8d). It is concluded that the C_8 tails of amphiphiles **1**, **2**, **3** are not long enough for formation of stable surface monolayers.

4. Conclusion

We concluded from these results that spontaneous assembling behavior of single-chain ammonium amphiphiles containing the benzylideneaniline or salicylideneaniline unit is essentially identical to that of azobenzene-containing ammonium amphiphiles. In the aqueous system, typical bilayer characteristics are observed for the former compounds, although their aggregate morphologies vary with their chemical structure. The azobenzene system has been extensively studied and the correlation between molecular structures and assembling patterns is now well established. The present results, therefore, endorse the validity of a more general correlation between molecular structure and mode of assembly. A major difference we found between the azobenzene system and the present system, was chemical stability. The azobenzene chromophore organized in bilayer assembly provides many unique features in the photochemical and photophysical behavior. Therefore, the generalized correlation is useful for designing novel functional materials.

Acknowledgement

The authors are grateful to Dr. *Kurihara* and Mr. *Yanagi* of Molecular Architecture Project ERATO, for surface monolayer measurements.

References

[1] Contribution No. 991 from Department of Chemical Science and Technology.
[2] *T. Kunitake* and *Y. Okahata*, J. Am. Chem. Soc. **99**, 3860 (1977).
[3] *T. Kunitake*, Angew. Chem., Int. Ed. Engl. **31**, 709 (1992).
[4] *T. Kunitake* and *Y. Okahata*, J. Am. Chem. Soc. **102**, 549 (1980).
[5] *T. Kunitake, Y. Okahata, M. Shimomura, S. Yasunami, K. Takarabe*, J. Am. Chem. Soc. **103**, 5401 (1981).
[6] *M. Shimomura, R. Ando, T. Kunitake*, Ber. Bunsenges. Phys. Chem. **87**, 1134 (1983).
[7] *T. Kunitake, M. Shimomura, T. Kajiyama, A. Honda, K. Okuyama, M. Takayanagi*, Thin Solid Films **121**, L89 (1984).
[8] *K. Okuyama, H. Watanabe, M. Shimomura, K. Hirabayashi, T. Kunitake, T. Kajiyama, N. Yasuoka*, Bull. Chem. Soc. Jpn. **59**, 3351 (1986).
[9] *G. Xu, K. Okuyama, M. Shimomura*, Mol. Cryst. Liq. Cryst. **213**, 105 (1991).
[10] *M. Shimomura* and *T. Kunitake*, J. Am. Chem. Soc. **109**, 5175 (1987).
[11] *N. Kimizuka* and *T. Kunitake*, Chem. Lett., 827 (1988).
[12] *H. Nakahara, K. Fukuda, M. Shimomura, T. Kunitake*, Nippon Kagaku Kaishi, 1001 (1988).
[13] *N. Kimizuka* and *T. Kunitake*, Colloid and Surface **38**, 79 (1989).
[14] *Y. Okahata, R. Ando, T. Kunitake*, Bull. Chem. Soc. Jpn. 802 (1983).
[15] *Y. Ishikawa, T. Nishimi, T. Kunitake*, Chem. Lett. 165 (1990).
[16] *T. Kunitake, R. Ando, Y. Ishikawa*, Memoirs Faculty Eng., Kyushu Univ. **46**, 221 (1986).
[17] *I. Teucher, C.M. Paleos, M.M. Labes*, Mol. Cryst. Liq. Cryst. **11**, 187 (1970).
[18] *M. Ottolenghi, D.S. McClure*, J. Chem. Phys. **46**, 4613 (1967).